

VLT/FORS2 observations of the optical counterpart of the isolated neutron star RBS 1774[★]

R. P. Mignani^{1,2}, S. Zane¹, R. Turolla^{3,1}, F. Haberl⁴, M. Cropper¹,
C. Motch⁵, A. Treves⁶, and L. Zampieri⁷

¹ Mullard Space Science Laboratory, University College London, Holmbury St. Mary, Dorking, Surrey, RH5 6NT, UK
e-mail: rm2@mssl.ucl.ac.uk

² Institute of Astronomy, University of Zielona Góra, Lubuska 2, 65-265 Zielona Góra, Poland

³ Department of Physics, University of Padua, via Marzolo 8, 35131 Padua, Italy

⁴ CNRS, Université de Strasbourg, Observatoire Astronomique, 11 rue de l'Université, 67000 Strasbourg, France

⁵ Max Planck Institut für Extraterrestrische Physik, Giessenbachstrasse, 85748 Garching, Germany

⁶ Dipartimento di Fisica e Matematica, Università dell'Insubria, via Valleggio 11, 22100 Como, Italy

⁷ INAF, Osservatorio Astronomico di Padova, Vicolo dell'Osservatorio 5, 35122 Padova, Italy

Received 20 December 2010 / Accepted 15 March 2011

ABSTRACT

Context. The X-ray observations performed with the Röntgen Satellite (ROSAT) have led to the discovery of a group (seven to date) of X-ray dim and radio-silent, middle-aged isolated neutron stars (a.k.a. XDINSs), which are characterised by pure blackbody spectra ($kT \approx 40\text{--}100$ eV) and long X-ray pulsations ($P = 3\text{--}12$ s), and appear to be endowed with relatively high magnetic fields, ($B \approx 10^{13}\text{--}10^{14}$ G). Optical observations of XDINSs are important, together with the X-ray ones, for studying the cooling of the neutron star surface and for investigating the relation between XDINSs and other isolated neutron star classes. RBS 1774 is one of the few XDINSs with a candidate optical counterpart, which we discovered with the Very Large Telescope (VLT).

Aims. We aim at constraining the optical spectrum of RBS 1774, for which only two *B*-band flux measurements are available, and to determine whether its optical emission has either a thermal or a non-thermal origin.

Methods. We performed deep observations of RBS 1774 in the *R* band with the VLT to disentangle a non-thermal power-law spectrum from a Rayleigh-Jeans, whose contributions are expected to be very different in the red part of the spectrum.

Results. We did not detect the RBS 1774 candidate counterpart down to a 3σ limiting magnitude of $R \sim 27$. The constraint on its colour, $(B - R) \lesssim 0.6$, rules out its being a background object, positionally coincident with the X-ray source. Our *R*-band upper limit is consistent with the extrapolation of the *B*-band flux (assuming a 3σ uncertainty) for a set of power laws $F_\nu \propto \nu^{-\alpha}$ with spectral indices $\alpha \leq 0.07$. If the optical spectrum of RBS 1774 were non-thermal, its power-law slope would be very much unlike those of all isolated neutron stars with non-thermal optical emission, suggesting that it is most likely thermal. For instance, a Rayleigh-Jeans with temperature $T_0 = 11$ eV, for an optically emitting radius $r_0 = 15$ km and a source distance $d = 150$ pc, would be consistent with the optical measurements. The implied low distance is compatible with the 0.04 X-ray pulsed fraction if either the star spin axis is nearly aligned with the magnetic axis or with the line of sight or it is slightly misaligned with respect to both the magnetic axis and the line of sight by $5\text{--}10^\circ$.

Conclusions. New observations, both from the ground and from the *Hubble* Space Telescope (HST), are important to characterise the optical/near-ultraviolet (UV) spectrum of RBS 1774, to better constrain the values of r_0 , d , and T_0 and measure the source's proper motion from which indirect constraints on the source distance can be inferred.

Key words. stars: neutron

1. Introduction

One of the most intriguing results of the all sky survey performed by the Röntgen Satellite (ROSAT) has been the discovery of seven X-ray dim and radio-silent, middle-aged isolated neutron stars (a.k.a. XDINSs, see Haberl 2007 and Turolla 2009, for the most recent reviews). XDINSs stand apart from most X-ray emitting INSs due to their pure blackbody X-ray spectra ($kT \approx 40\text{--}100$ eV), produced from the cooling of the neutron star surface. Shallow X-ray pulsations ($P = 3\text{--}12$ s), likely from large and hot polar caps, are observed for all but one of them. The measurement of the period derivative \dot{P} in some XDINSs (see Kaplan & van Kerkwijk 2009 and references

therein) yielded, if assuming magneto-dipolar spin-down, ages of $\sim 1\text{--}2$ Myr and rotational energy losses $\dot{E} \sim 2\text{--}5 \times 10^{30}$ erg s⁻¹, which is too small to power detectable magnetospheric emission. Interestingly, XDINSs appear to be endowed with relatively high magnetic fields, $B \approx 10^{13}\text{--}10^{14}$ G, as inferred from spin-down measurements and the detection of broad spectral features, which could be attributed to proton cyclotron scattering and/or electron transitions in H/He-like atoms. Besides the X-rays, XDINSs are only detected in the optical. In radio, stringent upper limits have been obtained at 820 MHz (Konradiev et al. 2009), while the detections of RX J1308.6+2127 and 1RXS J214303.7+065419 at 111 MHz (e.g. Malofeev et al. 2007) are still unconfirmed. XDINSs feature a ≥ 5 optical excess with respect to the extrapolation of the X-ray spectrum (see, e.g. Mignani 2011) and, at least in the two best-studied cases

[★] Based on observations collected at ESO, Paranal, under Programme 383.D-0485(A).

(RX J0720.4–3125 and RX J1856.5–3754), their optical fluxes closely follow a Rayleigh-Jeans (R-J) distribution, with a possible additional power-law (PL) component for the former (Kaplan et al. 2003). Whether the XDINSs optical emission is produced from regions of the star surface that are larger and cooler than those producing the X-rays (e.g. Pons et al. 2002) is debated.

1RXS J214303.7+065419 (a.k.a. RBS 1774) is the last of the ROSAT-discovered XDINS (Zampieri et al. 2001) and possibly that with the highest inferred magnetic field ($\approx 10^{14}$ G; Zane et al. 2005)¹. Recently, we observed this source with the Very Large Telescope (VLT), and we identified its optical counterpart ($B = 27.4 \pm 0.2$; Zane et al. 2008). Interestingly, the neutron star flux was found to be a factor ≈ 35 above the optical extrapolation of the *XMM-Newton* X-ray spectrum ($kT \sim 104$ eV; $N_{\text{H}} \sim 3.6 \times 10^{20}$ cm⁻²; Zane et al. 2005), and a slightly larger optical excess was measured with the Large Binocular Telescope (LBT) by Schwöpe et al. (2009). So far, nothing is known about the optical/IR spectrum of RBS 1774, for which only the two *B*-band flux measurements of Zane et al. (2008) and Schwöpe et al. (2009) are available. Prior to our detection of the optical counterpart, the neutron star was observed both at optical and infrared (IR) wavelengths (Lo Curto et al. 2007; Rea et al. 2007; Posselt et al. 2009), but no counterpart was found.

To constrain the optical spectrum of RBS 1774, we performed new observations with the VLT in the *R* band to disentangle the slope of a flat PL continuum from that of a *R* – *J* distribution and, thus, to determine whether the optical emission is non-thermal or thermal, i.e. associated either with the magnetosphere or the neutron star surface.

This paper is organised as follows: observations, data reduction, and analysis are described in Sect. 2, while results are presented and discussed in Sect. 3. Conclusions then follow.

2. Observations and data analysis

We obtained optical images of the RBS 1774 field with the VLT Antu telescope at the ESO Paranal observatory on September 19 and 20, 2009. Observations were performed in service mode with the FOCal Reducer/low dispersion Spectrograph (FORS2), a multi-mode camera for imaging and long-slit/multi-object spectroscopy (Appenzeller et al. 1998), using the default *R* *Special* filter ($\lambda = 6550$ Å; $\Delta\lambda = 1650$ Å). To achieve the highest sensitivity at longer wavelengths, FORS2 was equipped with its red-sensitive MIT detector, a mosaic of two $2\text{k} \times 4\text{k}$ CCDs optimised for wavelengths longer than 6000 Å. In its standard resolution mode, the detector has a pixel size of $0''.25$ (2×2 binning), which corresponds to a projected field-of-view of $8'.3 \times 8'.3$ over the CCD mosaic. However, due to vignetting, the effective sky coverage of the two detectors is smaller than the projected detector field-of-view, and it is larger for the upper CCD chip. To include more reference stars for a precise image astrometry, as well as to increase the signal-to-noise ratio per pixel, we performed the observations in standard resolution mode. We positioned RBS 1774 in the upper CCD chip to exploit its larger effective sky coverage ($7' \times 4'$). The instrument was operated in its standard low gain, fast read-out mode.

To allow for cosmic ray removal, a sequence of 20 exposures of 775 s each were obtained in the two nights, for a total integration time of 9300 s and 6200 s for the first and second nights,

¹ This value has been inferred from the observations of an absorption feature in the X-ray spectrum of the source. However, the recent measurement of the pulsar spin-down (Kaplan & van Kerkwijk 2009) implies a magnetic field of $\sim 2 \times 10^{13}$ G.

respectively. Exposures were taken in dark time and under photometric conditions, as recorded by the ESO ambient condition monitor² and close to the zenith, with an airmass mostly below 1.3. The image quality was not constant during our observations. The seeing values measured by the Paranal differential image motion monitor (DIMM) are relative to the zenith and not to the pointing direction of the telescope and are subject to ground-layer turbulence (see also Martínez et al. 2010). Thus, they are not necessarily indicative of the actual image quality. For this reason, we computed it from the measured point spread function (PSF), which was derived by fitting the full width half maximum (*FWHM*) of a number of well-suited field stars using the *SExtractor* tool (Bertin & Arnouts 1996), following the recipe used by the FORS2 data quality control procedures³. The average image quality in the first night was $\sim 0''.6$, while in the second night it was $\sim 0''.9$. Bias, twilight flat-field frames, and images of standard star fields (Landolt 1992) were obtained as part of the FORS2 science calibration plan.

Data were reduced through the ESO FORS2 data reduction pipeline⁴ for bias subtraction and flat-field correction. Photometric calibration was applied using the extinction-corrected night zero points computed by the FORS2 pipeline and available through the instrument's data quality-control database. We converted the FORS2 zero points, computed in units of electrons/s, to units of ADU/s by applying the corresponding electrons-to-ADU conversion factors. We finally co-added the reduced science images using the *IRAF* task *drizzle* and applying a 3σ filter on the single pixel average to filter out residual hot and cold pixels. To achieve a better signal-to-noise, we decided to use only the images taken on the first night, which have the best image quality in our sample and provide the longest integration time (9300 s). Of course, we verified that adding the images taken on the second night does not improve the signal-to-noise.

To locate the RBS 1774 candidate counterpart in our FORS2 image, we used its position measured in our original FORS1 observation as a reference. Since the FORS1 detector was also a mosaic of two $2\text{k} \times 4\text{k}$ CCDs (but blue-optimised), with the same pixel size and field-of-view as FORS2 at standard resolution, we decided to register the counterpart position on our co-added FORS2 image through a relative astrometry procedure. Whenever possible, this approach yields a position registration in the detector reference frame which is more accurate than can be achieved through absolute astrometry, since it is not affected by the intrinsic absolute accuracy of the reference catalogue we used. Moreover, most of the reference stars from e.g. the GSC-2 (Lasker et al. 2008) are saturated in our images. For our relative astrometry, we used the positions of several point-like objects detected in the field-of-view with *SExtractor* as a reference, after filtering out objects that are either saturated, too faint, or too close to the CCD edges. The relative frame registration was performed with standard tools available in *IRAF* and turned out to be accurate to better than 0.05 pixels ($\sim 0''.0125$) in both the *x* and *y* directions, which are aligned with right ascension and declination to better than 0.1° . To this, we added the uncertainty on the candidate counterpart centroid on the FORS1 image which is ~ 0.1 pixels ($\sim 0''.025$). Since the FORS1 position refers to July 11, 2007 (MJD = 54 292), we have to account for an additional positional uncertainty due to the unknown neutron star proper motion to the date of our FORS2 observations

² <http://archive.eso.org/asm/ambient-server>

³ www.eso.org/observing/dfo/quality/FORS2/qc/qc1.html

⁴ www.eso.org/observing/dfo/quality/FORS2/pipeline

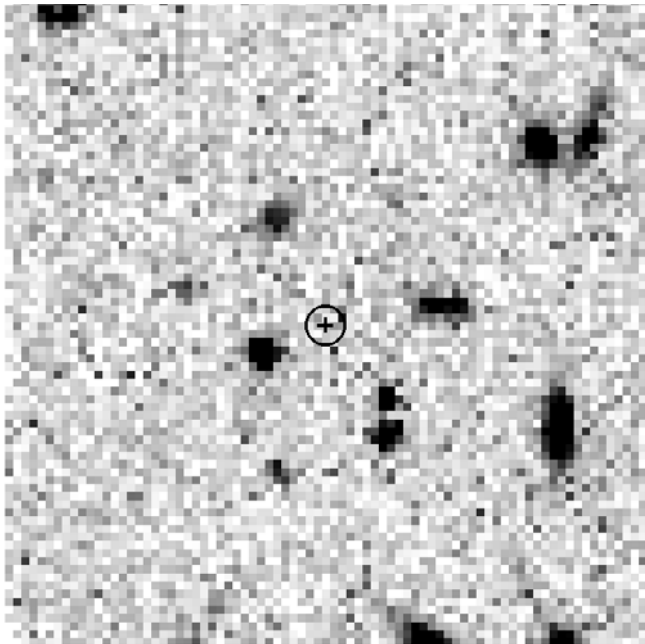


Fig. 1. VLT/FORS2 $20'' \times 20''$ co-added R -band image (9300 s integration time) of the RBS 1774 field (north to the top, east to the left). The computed position of the candidate counterpart is marked by the cross. For better visualisation, the cross arms ($0''.25$) are equal to 20 times the 1σ uncertainty of our relative astrometry. The circle ($\sim 0''.6$ radius) corresponds to the position uncertainty due to the unknown neutron star proper motion for, e.g. a transverse velocity of 400 km s^{-1} and a distance of 300 pc.

(MJD = 55 093). This corresponds to a yearly displacement of $\sim 0.2'' v_{100}/d_{100}$, where v_{100} and d_{100} are the unknown neutron star transverse velocity and distance⁵ in units of 100 km s^{-1} and 100 pc, respectively. For, e.g., an average neutron star velocity of $\sim 400 \text{ km s}^{-1}$ (Hobbs et al. 2005) and a distance of 300 pc, this would translate into an additional positional uncertainty of $\sim 0''.6$, which obviously dominates the uncertainty on our relative astrometry.

3. Results

3.1. Photometry

The computed position of the RBS 1774 candidate counterpart, overlaid on the co-added FORS2 R -band image, is shown in Fig. 1. As is apparent, no source can be visually identified at the expected neutron star position. We ran an automatic search with *SExtractor*, but did not detect any object above the 3σ detection threshold. We applied an image smoothing using a Gaussian function over 3×3 pixel cells, but we could not detect any new feature that could be unambiguously associated to a real object and not to an enhanced background fluctuation. Thus, we conclude that the optical counterpart of RBS 1774 is undetected in our images. We note that the $0''.6$ positional uncertainty shown in Fig. 1 corresponds to the assumed values of the neutron star distance (300 pc) and transverse velocity (400 km s^{-1}), so it is only indicative. However, our conclusions are not affected by the actual position uncertainty of the neutron star since no new object is detected within a radius of $5''$ from the nominal candidate counterpart position with respect to those already detected (see

Fig. 1 of Zane et al. 2008). We determined the detection limit of our FORS2 image from the number of counts corresponding to a 3σ detection in an aperture of a 2-pixel radius ($0''.5$), derived from the standard deviation of the background sampled around the expected neutron star position. We then corrected the number of counts for the airmass, using the atmospheric extinction coefficients measured for FORS2 and available through the instrument data quality control database, and we applied the aperture correction. The correction was computed from the measured growth curve of a number of relatively bright but unsaturated stars in the field, with no adjacent star closer than $5''$. Thus, their photometry is not affected by strong background gradients. The final 3σ limit of $R \sim 27$ is about 1.3 mag fainter than the r' upper limit reported by Rea et al. (2007).

Non having detected the Zane et al. (2008) candidate in our new VLT R -band images might cast some doubt on whether this object is indeed the optical counterpart of RBS 1774, although the low coincidence probability with the *Chandra* position (2×10^{-3} ; Zane et al. 2008) already made the association quite robust. Given the flux of the candidate counterpart ($B = 27.4 \pm 0.2$), not detecting it in the R band corresponds to an observed $(B - R) \lesssim 0.6$. The observed upper limit on the colour, together with the brightness of the candidate counterpart, can be used to rule out that this is a background object, positionally coincident with the neutron star. Since RBS 1774 coordinates point to quite a high galactic latitude ($l = 62.6556^\circ$, $b = -33.1392^\circ$), as shown by the many galaxies identified in the field, the candidate counterpart might, in principle, be an AGN. Indeed, most AGNs at $z \lesssim 2$ have $0 \lesssim (B - R) \lesssim 3$, which is compatible with the colour of the RBS 1774 candidate counterpart. That no transient/persistent radio source was detected at its position in recent, deep 840 MHz observations (Kondratiev et al. 2009) would only rule out a radio-loud AGN. However, an AGN not detected in X-rays⁶ would be either very absorbed or at a much higher redshift, which would hardly be compatible with the constraint on its $(B - R)$ or with its detection in the B band, respectively. On the other hand, a $(B - R) \lesssim 0.6$ would be compatible with a main sequence star of spectral type earlier than F, but this should be well outside the Galaxy to reproduce the observed B -band flux. Thus, both the counterpart colour and its brightness are only compatible with a neutron star.

3.2. Multi-band spectrum

We compared our R -band magnitude upper limit with the best-fit model to the *XMM-Newton* spectrum of RBS 1774 and with the available multi-band photometry (Rea et al. 2007; Zane et al. 2008; Schwöpe et al. 2009). We computed the interstellar extinction correction from the hydrogen column density N_{H} derived from the X-ray spectral fit. To this aim, we fitted the *XMM-Newton* spectrum anew using updated calibrations and response files. We extracted the EPIC-pn spectrum again from the original May 2004 observation using version 10.0.0 of the *XMM-Newton* Science Analysis System (SAS), a circular region of $20''$ radius, and selected only single-pixel events. Since combined fits with pn and MOS spectra are dominated by the higher statistical quality of the pn spectrum, we concentrated on the pn spectrum alone. For comparison with the results obtained by Schwöpe et al. (2009) and Cropper et al. (2007), we fitted the spectrum with either a black body (BB) model, a BB plus an (additive) Gaussian line, and a BB plus a (multiplicative) absorption

⁵ Posselt et al. (2009) quote a fiducial lower limit of 300 pc, estimated from models of the N_{H} distribution.

⁶ *Chandra* observations of RBS 1774 rule out a blend with a background X-ray source.

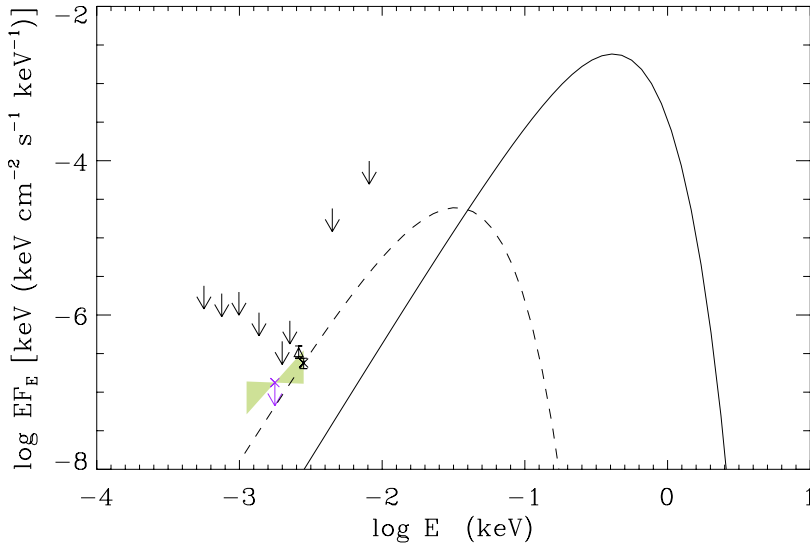


Fig. 2. Optical/X-ray spectral energy distribution of RBS 1774. The solid line represents the updated best-fit model spectrum ($kT \sim 104$ eV; $N_{\text{H}} \sim 2.6 \times 10^{20} \text{ cm}^{-2}$) to the *XMM-Newton* data. The arrows represent the 5σ optical/IR flux upper limits reported by Rea et al. (2007) and the 3σ near/far-ultraviolet flux upper limits derived from archival *GALEX* observations (see text). The VLT *B*-band flux of the RBS 1774 candidate counterpart is marked by the cross, while our VLT *R*-band upper limit is marked by the cross and the arrow. The *LBT* *B*-band measurement (Schwope et al. 2009) is marked by the triangle. The shaded areas represent the region described by the two PLs with slopes $\alpha = -2.07$ and 0.07 , which pass $\pm 3\sigma$ above/below the *B*-band flux and are consistent with our *R*-band upper limit (see text for details). Optical points have been corrected for the N_{H} obtained from the updated fit to the *XMM-Newton* spectrum (see text). The dashed line represents the blackbody at $T_0 = 11$ eV ($r_0 = 15$ km, $d = 150$ pc), normalised to our VLT *B* band point and compatible with the *R*-band upper limit.

Table 1. Best-fit parameters to the X-ray *XMM-Newton* spectrum computed for different models.

Model	N_{H} (10^{20} cm^{-2})	kT (eV)	E_{line} (eV)	σ_{line} (eV)	$\chi_r 2(\text{d.o.f.})$
(1) bbody	2.7 ± 0.2	102.0 ± 1.2	–	–	1.51 (133)
(2) bbody+gauss	2.6 ± 0.2	104.2 ± 2.1	728 ± 16	31 ± 31	1.20 (130)
(3) bbody*gauss	2.6 ± 0.2	104.1 ± 2.1	733 ± 17	31 ± 30	1.20 (130)

edge. In each case, interstellar absorption was included by using the XSPEC (version 12.6.0k) model *phabs* with abundances from Wilms et al. (2000). The best-fit parameters are summarised in Table 1. As in previous analyses, including an absorption feature improves the fit over a simple BB model, although the current energy resolution does not allow a Gaussian line in absorption to be distinguished from an edge. The slight differences between the model parameters reported here and those given by Schwope et al. (2009) and Cropper et al. (2007) are largely due to the different revisions of the soft spectral response calibration of the EPIC-pn camera and possibly different elemental abundances used for the absorption model. The new spectral fit with an absorbed BB plus an (additive) Gaussian line yields a best-fit temperature of $kT = 104.2 \pm 2.1$ eV, consistent with the one obtained by Zane et al. (2005) by fitting the same *XMM-Newton* data but with older calibrations and response files. However, we note that our new spectral fit yields a best-fit N_{H} value of $(2.6 \pm 0.2) \times 10^{20} \text{ cm}^{-2}$, which is somewhat lower than obtained by Zane et al. (2005), $N_{\text{H}} = 3.6 \times 10^{20} \text{ cm}^{-2}$, and which was used both in Rea et al. (2007) and in Zane et al. (2008) to compute the interstellar extinction. This resulted in slightly larger extinction-corrected fluxes, where the effect is ≤ 0.08 mag, i.e. well below the uncertainties on their absolute photometry. Nonetheless, in the following we assume $N_{\text{H}} = 2.6 \times 10^{20} \text{ cm}^{-2}$ as a reference, obtained from our updated spectral fits to the *XMM-Newton* spectrum. From this value, we derived an interstellar reddening $E(B - V) = 0.046$ using the relation of Predehl & Schmitt (1995)⁷. And, from this, we computed the interstellar

extinction in the different bands using the extinction coefficients of Fitzpatrick (1999). We then corrected the available multi-band photometry accordingly.

The new extinction-corrected multi-band fluxes from Rea et al. (2007), Zane et al. (2008), and Schwope et al. (2009) are shown in Fig. 2, together with the best-fit *XMM-Newton* spectrum and its extrapolation in the optical domain. To these points, we added flux measurements obtained in the near-ultraviolet (UV). The RBS 1774 field has been observed with the *GALEX* satellite (Martin et al. 2005) in both the NUV ($\lambda = 2771 \text{ \AA}$; $\Delta\lambda \sim 530 \text{ \AA}$) and FUV passbands ($\lambda = 1528 \text{ \AA}$; $\Delta\lambda \sim 220 \text{ \AA}$). We retrieved the fully reduced and calibrated imaging data from the *GALEX* archive⁸ for inspection, but we could not detect the source down to 3σ upper limits of $2.76 \mu\text{Jy}$ and $5.77 \mu\text{Jy}$ in the NUV and FUV passbands, respectively. We corrected these fluxes for the interstellar extinction using the $E(B - V) = 0.046$ derived above as a reference and the extinction coefficients of Fitzpatrick (1999) for the NUV passband and of Seaton (1979) for FUV one. The field has been also observed with the *XMM-Newton Optical Monitor* (Mason et al. 2001) in the *UWV1* ($\lambda = 2675 \text{ \AA}$; $\Delta\lambda \sim 577 \text{ \AA}$), *UWV2* ($\lambda = 2205 \text{ \AA}$; $\Delta\lambda \sim 350 \text{ \AA}$), and *UVW2* ($\lambda = 1894 \text{ \AA}$; $\Delta\lambda \sim 330 \text{ \AA}$) filters, but the source was not detected down to 3σ limits which are not deeper than the *GALEX*/NUV one. At shorter wavelengths, the source was not detected by *EUVE* during its all-sky scan and was not targeted by pointed observations (Bowyer et al. 1996). As seen from Fig. 2, the *GALEX* points lie at least two orders of

⁷ This relation is affected by uncertainties for close objects, due to the problems of modelling the interstellar medium (ISM) at a short distance from the Sun where microstructures weight more. We

checked that, when using the relations of Bohlin et al. (1978) and of Paresce (1984), extinction corrections are consistent within 0.04 mag, well below the pure statistical error on the source count rate.

⁸ www.galex.stsci.edu

magnitude above the X-ray spectrum extrapolation. Thus, they cannot be used to constrain the shape of the optical spectrum.

3.3. The optical excess

The extrapolation of the new best-fit spectrum in the optical domain lies a factor 1.35 above the extrapolation derived in Zane et al. (2008). Thus, as the result of the new fit to the *XMM-Newton* spectrum the optical excess of the VLT *B*-band flux is $\sim 24.4 \pm 3.7$ (1σ confidence level). This is lower than the value of 35 ± 7 (1σ) published in Zane et al. (2008), although still marginally consistent within 1σ errors. As shown in Sect. 3.2, the difference in the N_H obtained from our spectral fit and that of Zane et al. (2005) only corresponds to a difference of $\lesssim 0.08$ mag in the dereddened *B*-band flux. Thus, it only has a negligible effect on the lower optical excess that we derive, which is mainly from the difference in the extrapolation of the best-fit *XMM-Newton* spectrum, resulting from the use of new calibrations and response files. We also note that the value of the optical excess is insensitive to which of the two best-fit spectral models, (2) and (3) in Table 1, is actually assumed, since both the spectral parameters of the underlying blackbody and the inferred N_H are virtually identical. Schwobe et al. (2009) used LBT data to obtain a slightly brighter *B*-band magnitude of 26.96 ± 0.20 with respect to our value of $B = 27.4 \pm 0.2$ (Zane et al. 2008), which they interprets as a hint of a possible flux variability from the source. Taking the magnitude difference at face value, this would imply a difference of $\approx 50\%$ in the optical excess. However, the magnitude difference between the two measurements, 0.44 ± 0.28 (1σ error) is not statistically compelling. Moreover, the two measurements were made with different telescope/detectors and with unidentical filters, which brings in an additional uncertainty due to the colour-term correction, and were calibrated using different sets of standard stars, using default atmospheric extinction corrections. While Zane et al. (2008) applied the average *B*-band atmospheric extinction coefficient provided by ESO⁹ computed from observations performed at the Paranal Observatory over the April 2007–September 2007 semester with the same telescope/instrument set-up as was used in their own observations, Schwobe et al. (2009) applied the *B*-band extinction coefficients measured at the LBT site a few months apart, during the commissioning of the instrument. Since the measured atmospheric extinction coefficients can display a night-to-night scatter up to ~ 0.1 mag, this would introduce into both measurements an additional uncertainty of up to ~ 0.1 mag on the absolute photometry, for a target observed at the zenith, which is obviously larger if the target is observed at larger zenith angles. Accounting for all the above sources of uncertainties, the difference between the two *B*-band flux measurements is significantly smoothed out, and we regard them as consistent within the errors. Thus, in the following we use a value of the optical excess of $\sim 24.4 \pm 3.7$ as a reference, corresponding to our VLT *B*-band measurement.

4. Discussion

4.1. Non-thermal emission

Our new *R*-band magnitude upper limit corresponds to an unabsorbed spectral flux $< 1.33 \times 10^{-7}$ keV ($\text{keV cm}^{-2} \text{s}^{-1} \text{keV}^{-1}$), at a central energy of 1.77 eV. As seen from Fig. 2, the *R*-band upper limit is consistent with a set of PLs $F_\nu \propto \nu^{-\alpha}$ with spectral indices $-2.07 \leq \alpha \leq 0.07$, which pass $\pm 3\sigma$ above or below

⁹ www.eso.org/observing/dfo/quality/FORS1/qc/qc1.html

the *B*-band flux. If the optical spectrum of RBS 1774 were non-thermal, such a range of PLs would only be marginally compatible with the spectral indices measured for other types of isolated neutron stars with non-thermal optical emission, like the rotation-powered pulsars for which $0 \lesssim \alpha \lesssim 1$ (see Mignani et al. 2007b, 2010a,b). However, since the actual *R*-band flux of RBS 1774 is obviously below the derived upper limit, the PL would most likely have a negative spectral index, which makes the spectrum rise and not decline towards the near-UV. Thus, although we cannot rule out the presence of a PL component of non-thermal nature, we regard it as unlikely that the optical spectrum of RBS 1774 can be described by a single PL. Moreover, it is not clear what the origin of such a non-thermal PL could be. In Zane et al. (2008) we already deemed it unlikely that non-thermal optical emission from RBS 1774 can be powered by the neutron star rotational energy loss which, if of the order of $10^{30} \text{ erg s}^{-1}$ as observed in the other XDINSs, would imply an anomalously high optical emission efficiency, ~ 1000 times more than for rotation-powered pulsars (Zharikov et al. 2006). Alternatively, on the basis of a detection in only one band and without a deep upper limit in the *R* band, we suggested that non-thermal optical emission could be powered by the presumably large neutron star magnetic field ($\approx 10^{14}$ G; Zane et al. 2005), as proposed for the magnetars, whose optical/IR emission efficiency is also a factor of ≈ 1000 more for the radio pulsars (Mignani et al. 2007a). However, in the few cases where multi-band photometry is available, magnetar optical spectra are consistent with PLs with spectral index $\alpha \geq 0$, again very different from our limit for RBS 1774.

4.2. Thermal emission from the neutron star surface

The *R*-band upper limit is consistent with an *R* – *J* spectrum that passes through the *B*-band flux. A linear function connecting the VLT *B*-band point and the *R*-band upper limit has a slope ~ -1.26 , and the *R*-band upper limit lies only $\sim 25\%$ above the extrapolation of the *R* – *J* spectrum that passes through the central value of the measured *B*-band flux. This is compatible with both the *B* and *R*-band fluxes being on the same *R* – *J* spectrum, conceivably emitted by a region of the star surface, which is colder than the one responsible for the X-ray emission.

As in Zane et al. (2008), we consider a picture in which the optical emission originates in a colder fraction of the neutron star surface, which emits a blackbody spectrum at a temperature T_O (Braja & Romani 2002; Pons et al. 2002; Kaplan et al. 2003; Trümper et al. 2004). In the *R* – *J* tail, the ratio between the optical and X-ray fluxes scales as $\approx r_O^2 T_O / r_X^2 T_X \equiv f$, where r_O is the size of the optically emitting region (which, of course, cannot exceed the value of the neutron star radius), while r_X and T_X are the radius and temperature of the X-ray emitting region, as inferred from X-ray spectroscopy, $T_X = 104$ eV, $r_X = 2(d/300 \text{ pc}) \text{ km}$. Since the RBS 1774 distance is unknown, we iterated our computations over several values of d and r_O and derived the value of T_O that corresponds to a given value of the optical excess, f (as computed from the *B*-band flux). Since no contribution from such a cold component is observed in the 0.1–1 keV *XMM-Newton* spectrum¹⁰, it must be $R \ll 1$, where

$$R = \left(\frac{r_O}{r_X}\right)^2 \left(\frac{T_O}{T_X}\right)^4 \frac{\int_{0.1/T_O}^{1/T_O} t^3 / [\exp(t) - 1] dt}{\int_{0.1/T_X}^{1/T_X} t^3 / [\exp(t) - 1] dt}. \quad (1)$$

¹⁰ A soft thermal component to the X-ray spectrum could be compatible with the *XMM-Newton* RGS data, which show emission excess at low energies (Schwobe et al. 2009)

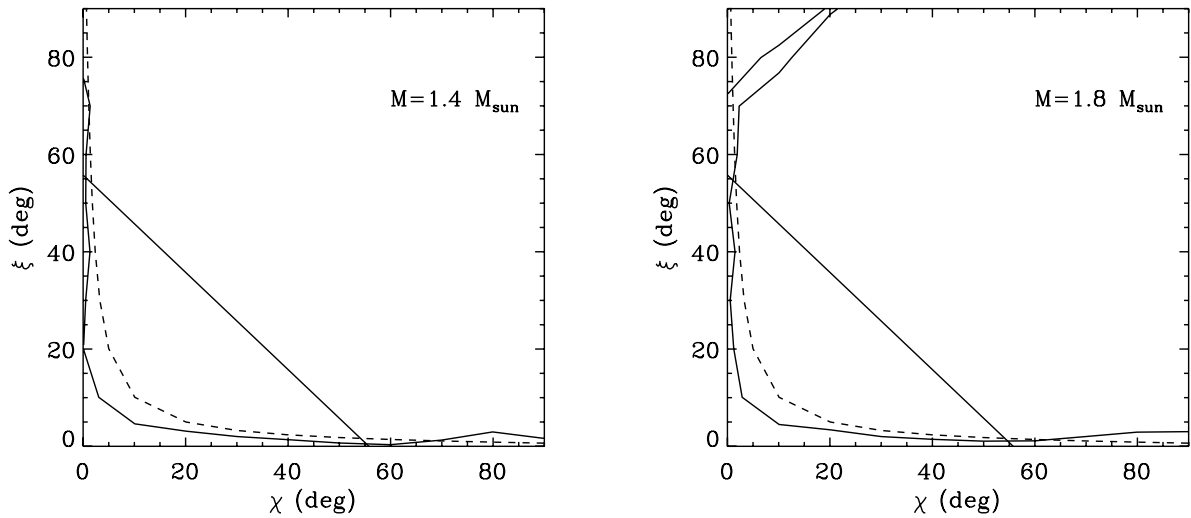


Fig. 3. *Left:* the contour of constant $PF=0.04$ (solid line) for the case $r_0 = 15$ km, $d = 150$ pc, $T_0 = 11$ eV, $r_X = 1$ km, and $M = 1.4 M_\odot$. The dashed line shows the analytical result for point-like caps (see text for details). Pulse profiles are class I according to the classification of Beloborodov (2002); i.e., they do not exhibit flat intervals, only when the contour is below the straight line. *Right:* same for $M = 1.8 M_\odot$.

Furthermore, the extrapolation of the cold blackbody component in the R band must be compatible with our new VLT upper limit. We performed the calculation for a large set of parameters, varying the source distance between 100 and 500 pc, the B -band excess f within the 3σ limits ($13.3 \leq f \leq 35.5$), and considering $r_0 = 10, 15,$ and 20 km¹¹. We found that the data are quite constraining: a radius $r_0 = 15$ km is compatible with the considered range of f only for $d \leq 200$ pc (which implies $r_X \leq 1.3$ km) and $T_0 \leq 20$ eV. Assuming a smaller radius ($r_0 = 10$ km), the observed excess is only compatible with even shorter distances (~ 100 pc, corresponding to $r_X = 0.6$ km) and $T_0 \leq 10$ eV. On the other hand, if assuming a larger radius ($r_0 = 20$ km), the observed excess is compatible with distances up to 300 pc (corresponding to $r_X \leq 2$ km) and $T_0 \leq 15$ eV. As an example, we plotted in Fig. 2 a blackbody with $T_0 = 11$ eV, corresponding to $r_0 = 15$ km and $d = 150$ pc.

Next, we verified if the inferred size of the hotter caps is compatible with the observed pulsed fraction (PF)

$$PF = \frac{2(F_{\max} - F_{\min})}{(F_{\max} + F_{\min})} \sim 0.04 \quad (2)$$

where F_{\max} (F_{\min}) are the maximum (minimum) value of the flux along the pulse. The PF was computed numerically by means of an IDL script for different allowed combinations of r_0 , r_X , and T_0 (that is, for which the condition $R \ll 1$ was met) and assuming in all cases $T_X = 104$ eV. We also used two values of the star mass, $M = 1.4, 1.8 M_\odot$ to check how sensitive our results are to general relativistic effects (which depend on the compactness M/R ; e.g. Beloborodov 2002). Since it is always $r_X \leq 0.1r_0$, we took the latter to coincide with the star radius. Results are shown in Fig. 3, where the curve of constant PF (0.04) is plotted as a function of the two geometrical angles, ξ , the angle between the neutron star spin and magnetic axes, and χ , the angle between the spin axis and the line-of-sight (LOS), for the case reported in Fig. 2. Overplotted to the numerical contour is the analytical curve that is obtained following the method presented by Beloborodov (2002) and which is strictly valid only

for point-like caps. The present analysis confirms previous findings (Zane et al. 2008; Schwope et al. 2009). One possibility is that either the spin axis is nearly aligned with the magnetic axis, hence the star is a nearly aligned rotator, or the spin axis is nearly aligned with the LOS. The other possibility is that the spin axis is slightly misaligned with respect to both the magnetic axis and the LOS by $5\text{--}10^\circ$. We note that, although the numerical and analytical curves are qualitatively similar there are quantitative differences. The allowed range in the two angles is somehow narrower in the complete calculation, as expected when the finite (albeit small) size of the caps is accounted for. This may also explain the somehow different conclusions reached by Schwope et al. (2009), who used a treatment that is only valid for point-like caps. The small opening of the X-ray emitting regions does not constrain the geometry too much, and several combinations of the angles ξ and χ are possible.

5. Summary and conclusions

We performed deep optical observations of RBS 1774 in the R band with FORS2 at the VLT to obtain the first characterisation of its optical spectrum. We did not detect the RBS 1774 candidate counterpart at its expected position down to a 3σ limiting magnitude of $R \sim 27$. The constraint on the colour of the candidate counterpart, $(B - R) \lesssim 0.6$, rules out a foreground object, positionally coincident with the X-ray source. We re-analysed the *XMM-Newton* data of RBS 1774 using new calibrations and response files (see Sect. 3.2). We found that the optical excess of the VLT B -band flux (Zane et al. 2008) with respect to the best-fit X-ray spectrum extrapolation is now 24.4 ± 11.1 (3σ confidence level). This value is still incompatible with rotation-powered non-thermal emission from RBS 1774, unless its optical emission efficiency is ~ 1000 times higher than that of rotation-powered pulsars (Zharikov et al. 2006). Moreover, our R -band upper limit would most likely imply a PL spectral index $\alpha < 0$, while rotation-powered pulsars usually have $0 \leq \alpha \leq 1$ (Mignani et al. 2007b; 2010a,b). On the other hand, explaining the optical excess in terms of pure thermal emission from the neutron star surface would require both a short distance and

¹¹ Neutron star radii of ≥ 20 km are unlikely for most equations of state (e.g., Lattimer & Prakash 2004).

rather stringent limits on the inclination of the LOS and the magnetic axis with respect to the neutron star spin axis. For instance, a radius $r_O \leq 15$ km implies a neutron star distance $d \leq 200$ pc, which implies $T_O \leq 20$ eV and $r_X \leq 1.3$ km. Such a small X-ray emitting area is compatible with the ~ 0.04 X-ray pulsed fraction if either the star spin axis is closely aligned with the magnetic axis or with the LOS or it is slightly misaligned with respect to both the magnetic axis and the LOS by $5\text{--}10^\circ$. Observations in the near-UV would obviously be crucial for constraining the slope of the RBS 1774 optical spectrum and for better constraining T_O and r_O . With the GALEX fluxes falling well above all possible $R - J$ spectra compatible with the VLT flux measurements, only the *Hubble* Space Telescope (HST) can provide the required near-UV sensitivity. Future optical observations, both from the ground and from space, will also be important for measuring the source's proper motion, for independently confirming the optical identification, and for inferring indirect constraints on the distance.

Acknowledgements. R.P.M. thanks the ESO User Support Department and the Paranal Science Operation team for support in the scheduling and execution of the VLT observations.

References

- Appenzeller, I., Fricke, K., Fürtig, W., et al. 1998, *The Messenger*, 94, 1
 Beloborodov, A. M. 2002, *ApJ*, 566, L85
 Bertin, E., & Arnouts, S. 1996, *A&AS*, 117, 393
 Bohlin, R. C., Savage, B. D., & Drake, J. F. 1978, *ApJ*, 224, 132
 Bowyer, S., Lampton, M., Lewis, J., et al. 1996, *ApJS*, 102, 129
 Braje, T. M., & Romani, R. W. 2002, *ApJ*, 580, 1043
 Cropper, M., Zane, S., Turolla, R., et al. 2007, *Ap&SS*, 308, 161
 Fitzpatrick, E. L. 1999, *PASP*, 111, 63
 Geppert, U., Küker, M., & Page, D. 2006, *A&A*, 457, 937
 Haberl, F. 2007, *Ap&SS*, 308, 181
 Hobbs, G., Lorimer, D. R., Lyne, A. G., & Kramer, M. 2005, *MNRAS*, 360, 974
 Kaplan, D. L., & van Kerkwijk, M. H. 2009, *ApJ*, 692, L62
 Kaplan, D. L., van Kerkwijk, M. H., Marshall, H. L., et al. 2003, *ApJ*, 590, 1008
 Kondratiev, V. I., McLaughlin, M. A., & Lorimer, D. R., et al. 2009
 Landolt, A. U. 1992, *AJ*, 103, 340
 Lasker, B. M., Lattanzi, M. G., McLean, B. J., et al. 2008, *AJ*, 136, 735
 Lattimer, J. M., & Prakash, M. 2004, *Science*, 304, 536
 Lo Curto, G., Mignani, R. P., Perna, R., et al. 2007, *A&A*, 473, 539
 Malofeev, V. M., Malov, O. I., & Teplykh, D. A. 2007, *Ap&SS*, 308, 211
 Martin, D. C., Fanson, J., Schiminovich, D., et al. 2005, *ApJ*, 619, L1
 Martinez, P., Kolb, J., Sarazin, M., & Tokovinin, A. 2010, *The Messenger*, 141, 3
 Mason, K. O., Breeveld, A., Much, R., et al. 2001, *A&A*, 365, L36
 Mignani, R. P. 2011, *AdSpR*, 47, 1281
 Mignani, R. P., Perna, R., Rea, N., et al. 2007a, *A&A*, 471, 265
 Mignani, R. P., Zharikov, S., & Caraveo, P. A. 2007b, *A&A*, 473, 891
 Mignani, R. P., Sartori, A., De Luca, A., et al. 2010a, *A&A*, 515, 110
 Mignani, R. P., Pavlov, G. G., & Kargaltsev, O. 2010b, *ApJ*, 720, 1635
 Paresce, F. 1984, *AJ*, 89, 1022
 Pons, J. A., Walter, F. M., Lattimer, J. M., et al. 2002, *ApJ*, 564, 981
 Posselt, B., Neuhäuser, R., & Haberl, F. 2009, *A&A*, 496, 533
 Predehl, P., & Schmitt, J. H. M. M. 1995, *A&A*, 293, 889
 Rea, N., Torres, M. A. P., Jonker, P. G., et al. 2007, *MNRAS*, 379, 1484
 Schwöpe, A., Erben, T., Kohnert, J., et al. 2009, *A&A*, 499, 267
 Seaton, M. J. 1979, *MNRAS*, 187, 73
 Trümper, J. E., Burwitz, V., Haberl, F., & Zavlin, V. E. 2004, *Nucl. Phys. B Proc. Suppl.*, 132, 560
 Turolla, R. 2009, *ASSL*, 357
 Wilms, J., Allen, A., & McCray, R. 2000, *ApJ*, 542, 914
 Zane, S., Cropper, M., Turolla, R., et al. 2005, *ApJ*, 627, 397
 Zane, S., Mignani, R. P., Turolla, R., et al. 2008, *ApJ*, 682, 487
 Zampieri, L., Campana, S., Turolla, R., et al. 2001, *A&A*, 378, L5
 Zharikov, S., Shibanov, Yu., & Komarova, V. 2006, *AdSpR*, 37, 1979